AIP | Review of Scientific Instruments

A two-dimensional polarization interferometry based parallel scan angular surface plasmon resonance biosensor

Le Liu, Suihua Ma, Yanhong Ji, Xinyuan Chong, Zhiyi Liu, Yonghong He, and Jihua Guo

Citation: Review of Scientific Instruments **82**, 023109 (2011); doi: 10.1063/1.3553028
View online: http://dx.doi.org/10.1063/1.3553028
View Table of Contents: http://scitation.aip.org/content/aip/journal/rsi/82/2?ver=pdfcov
Published by the AIP Publishing

A two-dimensional polarization interferometry based parallel scan angular surface plasmon resonance biosensor

Le Liu,[1] Suihua Ma,[1] Yanhong Ji,[2,a)] Xinyuan Chong,[1] Zhiyi Liu,[1] Yonghong He,[1,a)] and Jihua Guo[1]
[1]*Laboratory of Optical Imaging and Sensing, Graduate School at Shenzhen, Tsinghua University, Shenzhen 518055, China*
[2]*MOE Key Laboratory of Laser Life Science & Institute of Laser Life Science, South China Normal University, Guangzhou 510631, China*

(Received 11 May 2010; accepted 17 January 2011; published online 22 February 2011)

We describe a two-dimensional polarization interferometry based parallel scan angular surface plasmon resonance (SPR) biosensing technique. The method of line-shaped light illumination and parallel scan offers a high throughput. The simultaneous record of SPR angular spectrum enables the system to be unaffected by the time-dependent variation of the light source. The polarization interferometry technique lowers the minimum of the SPR dip and thereby reduces the noise related to the light intensity. Refractive index resolutions of 1.4×10^{-6} refractive index unit (RIU) under normal condition and 4.6×10^{-7} RIU under a more time-consuming condition are achieved in our angle interrogation based sensor. Meanwhile, a manually prepared DNA microarray has been detected, showing the potential applications of this technique in microarray analysis. © *2011 American Institute of Physics*. [doi:10.1063/1.3553028]

I. INTRODUCTION

Surface plasmon resonance (SPR) is a sensitive label-free sensing technique that has been widely used by biology and chemistry researchers.[1] In the past decade, SPR biosensors have become a central tool for characterizing and quantifying biomolecular interactions.[2] Recently, more and more two-dimensional SPR sensors have been developed for label-free detection of microarrays (also known as biochip).[3]

SPR sensors can be classified into four types of interrogation: intensity, phase, wavelength, and angle. Figure 1 shows the simulated relationships between the output and the refractive index (RI) of the analyte in these four types of SPR sensors.

In a SPR sensor based on intensity interrogation, a collimated beam of monochromatic light passes through a prism coupler, and the reflected beam is then recorded by a detector.[1,5,6] However, as the measured reflection intensity does not linearly depend on the refractive index [Fig. 1(a)], the technique offers a narrow dynamic range and a limited resolution (10^{-5} refractive index units (RIU) for both point sensing and two-dimensional sensing[1,5,6]). The sensitivity decreases outside the dynamic range. Furthermore, two different refractive indices may correspond to the same reflection intensity [Fig. 1(a)].

SPR sensors based on phase interrogation detect the variation of the refractive index by measuring the phase shift when SPR occurs [Fig. 1(b)]. The best reported refractive index resolution of this type of SPR sensors is 5.5×10^{-8} RIU for point sensing.[7] However, its sensitivity heavily relies on the thickness of the metal film, leading to a worse resolution for two-dimensional sensing (8.8×10^{-7} RIU).[8] Moreover, the dynamic range of SPR sensors based on phase interrogation is very narrow [Fig. 1(b)]. These drawbacks have limited the applications of the technique.

In a spectral SPR sensor (including wavelength and angle interrogation), the wavelength or angular spectrum is measured, and the sensor output is related to a change in the wavelength or angular position of the SPR dip. Compared with SPR sensors based on intensity and phase interrogation, the output of a spectral SPR sensor depends on the refractive index more linearly, and the dynamic range is much wider [Figs. 1(c) and 1(d)]. The refractive index resolutions of the point sensing SPR sensors based on wavelength and angle interrogation are in the order of 10^{-7} RIU.[9,10] Yuk *et al.*[11] and our group[12] have, respectively, reported SPR two-dimensional sensors based on wavelength interrogation with the refractive index resolution in the order of 10^{-5} RIU. Compared with SPR sensors based on wavelength interrogation, the output of the sensors with angular interrogation depends more linearly on the refractive index, as shown in Figs. 1(c) and 1(d). Lokate *et al.*[13] have reported a two-dimensional SPR biosensing technique based on angle interrogation, in which multiple images were used to calculate the SPR resonance angle (θ_{SPR}, the angle affording the minimum intensity). However, as the SPR angular spectrum curves are not recorded simultaneously, the variation of CCD imaging or the light source would increase the noise level and deteriorate the resolution.

The main noise deteriorating the resolution of spectral SPR sensors is proportional to the light intensity or the square root of it.[2] Metal film with ideal thickness can provide SPR dip whose minimum is nearly zero. But owing to precision and uniformity of the film coating, the minimum of the SPR dip is often much larger than zero, resulting in a considerable noise level. Methods to lower the minimum of the SPR dip by use of the phase difference between two polarization components when SPR occurs have been reported.[14] Our group has

a)Authors to whom correspondence should be addressed. Electronic addresses: jiyh@scnu.edu.cn and heyh@sz.tsinghua.edu.cn. Tel.: +86-755-26036395.

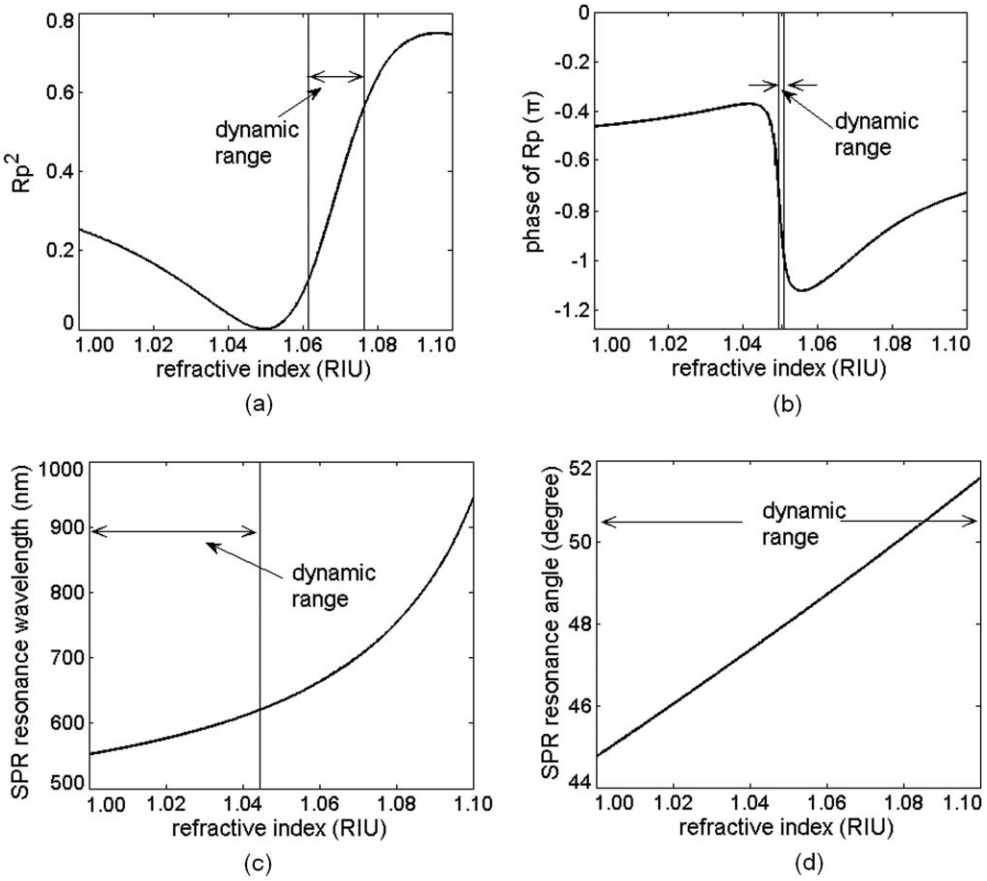

FIG. 1. Output and dynamic range comparison of four types of SPR sensors. [(a)–(d)] The simulated relationships between the output and the refractive index of the analyte in the SPR sensors based on intensity, phase, wavelength, and angle interrogation, respectively. Calculations are based on Fresnel's equations (Ref. 4) with Kretschmann configuration (Ref. 1), and the parameters are BK7 glass prism coated with 2 nm Cr and 40 nm Au films, the analyte of air, wavelength of 632.8 nm in (a), (b), and (d), incident angle of 48° in (a), (b), and (c). R_p is the reflection coefficient of the *p*-polarized light.

also reported a SPR sensor involving this technique, which we called "polarization interferometry (PI)."[15]

In this paper, we present for the first time, in so far as we know, a two-dimensional polarization interferometry based parallel scan angular SPR biosensing method. We experimentally demonstrate, with a line-shaped light illumination, that an image acquired with area CCD detector provides both SPR angular spectrum information and a one-dimensional spatial distribution. Thus a two-dimensional distribution of the refractive index on the entire sensing plane can be obtained with a one-dimensional optical line parallel scan. As the SPR angular spectrum is recorded simultaneously, the time-dependent variation of the light source does not increase the sensor noise. Furthermore, PI technique is employed in our system to reduce the noise, resulting in an improved resolution. Finally, we demonstrate the application of the system by detecting a manually prepared DNA microarray.

II. EXPERIMENTAL SYSTEM

A. System setup

The schematic of a polarization interferometry based parallel scan angular SPR imaging sensor is shown in Fig. 2(a). Light from a red light-emitting diode (LED) (A, 3 W power, central wavelength 632.8 nm) is focused by a 10× objective lens (B) on a pinhole (C) and then collimated by a collimation lens (D). The collimated light beam passes a bandpass filter (E, central wavelength 632.8 nm, bandwidth 10 nm) and is polarized by a linear glass polarizer (F, extinction ratio 500:1). After passing through a cylindrical convex lens with a vertical axis of symmetry (G), the light is focused into a vertical narrow line (H4) to irradiate the SPR module (H). The SPR module is configured in a Kretschmann manner with an attenuated total reflection method: a right angle prism (H1, BK7 glass, RI is 1.515) is coated with a Cr adhesive layer and a gold film (H2) on the hypotenuse plane (or be adhered to a Cr/Au film-coated glass sheet with refractive index matching oil on the hypotenuse plane) to excite SPR. Samples such as DNA microarray (H3) are prepared on the surface of the gold film. The prism is fixed on a one-dimensional translation stage that allows the sensing layer to move in the plane of the sample, orthogonal to the incident line-shaped beam. Thus we can scan the sample with the line-shaped beam by moving the one-dimensional translation stage. The reflected light beam is then collimated by a cylindrical convex lens with a vertical axis of symmetry (I), after which the light beam passes a quarter-wave plate (J) and another polarizer (K, the same model as F) in turn. Another cylindrical convex lens with a horizontal axis of symmetry (L) is used to image the

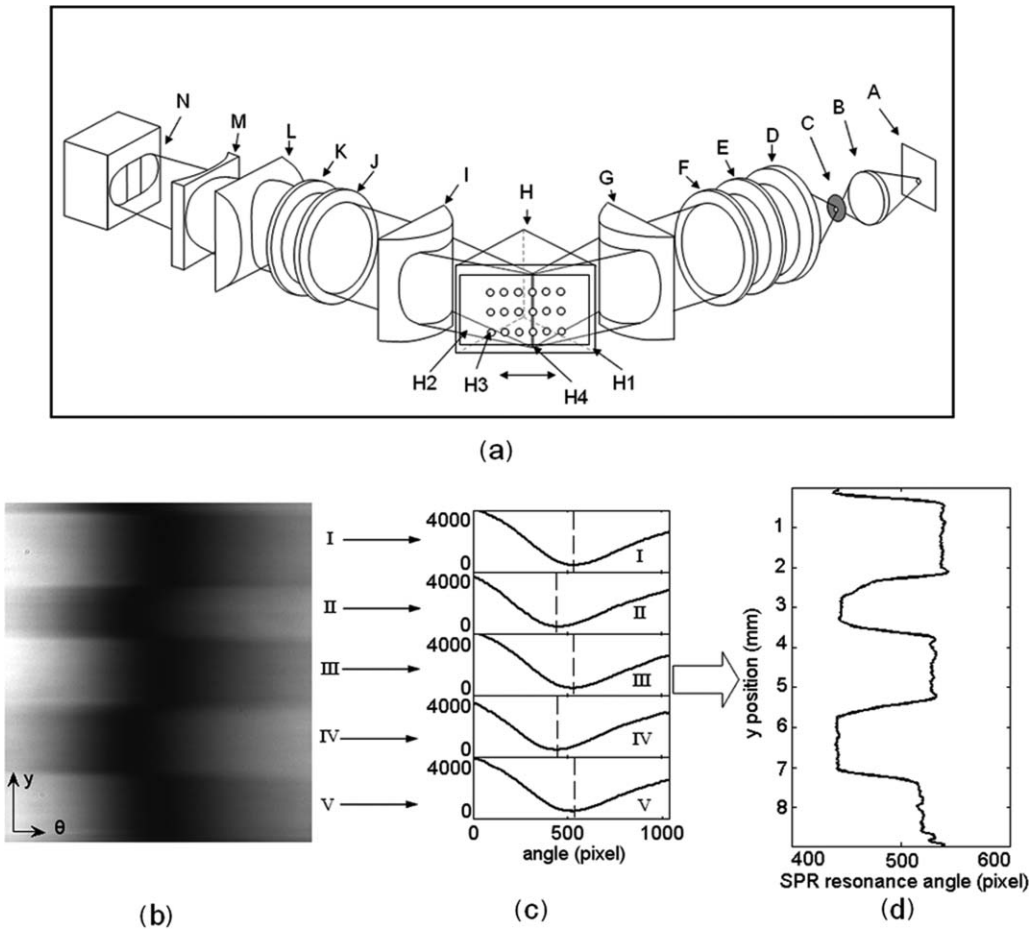

FIG. 2. (a) The schematic of a polarization interferometry based parallel scan angular SPR imaging sensor, A: LED light source, B: 10× objective lens, C: pinhole, D: collimation lens, E: bandpass filter, F: polarizer, G: cylindrical convex lens, H: Kretschmann-type SPR module (H1: prism, H2: gold film, H3: microarray, and H4: line-shaped beam), I: cylindrical convex lens, J: quarter-wave plate, K: polarizer, L: cylindrical convex lens, M: cylindrical concave lens, and N: CCD camera. (b) A typical image captured by the CCD with absence of quarter-wave plate J and polarizer K in (a), when the line-shaped beam crosses the spots of a microarray [such as H4 in (a)] after compensating the nonuniformity of the angular density caused by the light path. Areas I, III, and V are the spots of a microarray, areas II and IV are the bare gold film. (c) Five plotted rows from each area in (b) after five rows averaged. (d) The SPR resonance angle (which affording the minimum intensity) of a line area on the sensing plane represented by the image in (b).

sample irradiated by the line-shaped beam on the gold film. Then a cylindrical concave lens with a vertical axis of symmetry (M) is placed to expand the beam in the horizontal plane to enhance the angular resolution of the system. At the end of the light path is a CCD camera (N, Q-imaging RETIGA EXi 1394), which is controlled by a personal computer to acquire digitized images with a dynamic range of 12 bits and a resolution of 1392 × 1040 pixels.

An image captured by the CCD without PI technique [with absence of quarter-wave plate J and polarizer K in Fig. 2(a)] contains both SPR angular spectrum information and distribution information in one dimension. Figure 2(b) shows such an image when the line-shaped beam crosses the spots on a microarray [such as H4 in Fig. 2(a)] after compensating for the nonuniformity of the angular density caused by the light path. In Fig. 2(b), the five different areas marked with I–V correspond to either the spots of a microarray (areas I, III, and V) or the bare gold film (areas II and IV). We average each of the five adjacent rows of the image in Fig. 2(b) to reduce noise, which are plotted in Fig. 2(c). It can be seen that each curve in Fig. 2(c) represents a SPR angular spectrum with a SPR dip corresponding to one point on the sensing layer. Moreover, there is a position shift of the SPR dip of the microarray spots in comparison with that of the bare gold film. By applying tenth order polynomial curve fitting, we can calculate the angle affording the minimum intensity (SPR resonance angle) of a line represented by the image in Fig. 2(b). The angle value was shown in Fig. 2(d).

As the SPR resonance angle depends approximately linearly on the refractive index, we can obtain the refractive index information of a line from the image as shown in Fig. 2(b). By moving the translation stage and scanning the sample with the line-shaped beam, a series of images can be captured with the CCD. As a result, we can obtain the refractive index distribution information of the scanned area on the sensing layer.

In contrast with Lokate *et al.*'s technique, the SPR angular spectra of every line area can be measured simultaneously by taking our approach. So the time related noise (such as the intensity fluctuation of the light source) during the scan does not affect the RI resolution, but only affect the SPR angular spectra between different lines (e.g., the intensity

fluctuation of the light source will cause an offset of the SPR spectrum). This has little influence on the position of the SPR dip, so does not affect the spatial uniformity of the RI measurement.

It can be concluded from Fig. 2(c) that the minimum of the SPR dip is much greater than zero, resulting in a noise that cannot be totally eliminated by averaging adjacent rows. To reduce the minimum of the dip in the SPR angular spectrum, a quarter-wave plate [J in Fig. 2(a)] and another polarizer [K in Fig. 2(a)] are used to realize PI technique, which will be introduced in Sec. II B.

B. Polarization interferometry

Polarizer F, quarter-wave plate J, and polarizer K in Fig. 2(a) are used to realize PI technique. We use Jones matrix to analyze the principle. The polarized light after polarizer F can be represented by Jones vector

$$\begin{pmatrix} \cos\alpha \\ \sin\alpha \end{pmatrix}, \tag{1}$$

where α is the angle of polarized orientation of F with respect to p direction. The SPR module is represented by Jones matrix

$$\begin{pmatrix} r_p(\theta)e^{i\varphi_p(\theta)} & 0 \\ 0 & r_s(\theta)e^{i\varphi_s(\theta)} \end{pmatrix}, \tag{2}$$

where $r_p(\theta)$, $r_s(\theta)$, $\varphi_p(\theta)$, and $\varphi_s(\theta)$ are the amplitude and phase of reflection coefficient of p and s polarizations, and θ is the incident angle. The Jones matrix of the quarter-wave plate J, whose fast axis is at a 45° angle to p direction, is given by

$$\frac{1}{\sqrt{2}}\begin{pmatrix} 1 & i \\ i & 1 \end{pmatrix}. \tag{3}$$

The Jones matrix of polarizer K is

$$\begin{pmatrix} \cos^2\beta & \cos\beta\sin\beta \\ \cos\beta sin\beta & \sin^2\beta \end{pmatrix}, \tag{4}$$

where β is the angle of polarized orientation of K with respect to p direction. So the Jones vector of the light after polarizer K is

$$\begin{aligned}\begin{pmatrix} A \\ B \end{pmatrix} &= \begin{pmatrix} \cos^2\beta & \cos\beta\sin\beta \\ \cos\beta\sin\beta & \sin^2\beta \end{pmatrix}\frac{1}{\sqrt{2}}\begin{pmatrix} 1 & i \\ i & 1 \end{pmatrix} \\ &\quad \begin{pmatrix} r_p(\theta)\exp^{i\varphi_p(\theta)} & 0 \\ 0 & r_s(\theta)\exp^{i\varphi_s(\theta)} \end{pmatrix}\begin{pmatrix} \cos\alpha \\ \sin\alpha \end{pmatrix} \\ &= \frac{1}{\sqrt{2}}\begin{pmatrix} \cos^2\beta & \cos\beta\sin\beta \\ \cos\beta\sin\beta & \sin^2\beta \end{pmatrix} \\ &\quad \begin{pmatrix} r_p(\theta)\exp^{i\varphi_p(\theta)}\cos\alpha + ir_s(\theta)\exp^{i\varphi_s(\theta)}\sin\alpha \\ r_s(\theta)\exp^{i\varphi_s(\theta)}\sin\alpha + ir_p(\theta)\exp^{i\varphi_p(\theta)}\cos\alpha \end{pmatrix}.\end{aligned} \tag{5}$$

With adjustment of polarizer F, the condition of

$$\tan\alpha = \frac{r_p(\theta)}{r_s(\theta)} \tag{6}$$

can be fulfilled. If we define

$$r_p(\theta)\cos\alpha = r_s(\theta)\sin\alpha = C, \tag{7}$$

Eq. (5) can be reduced to

$$\begin{aligned}\begin{pmatrix} A \\ B \end{pmatrix} &= \frac{1}{\sqrt{2}}C\begin{pmatrix} \cos^2\beta & \cos\beta\sin\beta \\ \cos\beta\sin\beta & \sin^2\beta \end{pmatrix}\begin{pmatrix} e^{i\varphi_p(\theta)} + ie^{i\varphi_s(\theta)} \\ e^{i\varphi_s(\theta)} + ie^{i\varphi_p(\theta)} \end{pmatrix} \\ &= \sqrt{2}C\cos\left(\frac{\varphi_p(\theta)-\varphi_s(\theta)}{2} + \beta - \frac{\pi}{4}\right)e^{i((\varphi_p(\theta)-\varphi_s(\theta)/2)+(\pi/4))}\begin{pmatrix} \cos\beta \\ \sin\beta \end{pmatrix}.\end{aligned} \tag{8}$$

The two elements A and B of the Jones vector could be zero if we have

$$\frac{\varphi_p(\theta)-\varphi_s(\theta)}{2} + \beta - \frac{\pi}{4} = \frac{\pi}{2}, \tag{9}$$

i.e.,

$$\beta = \frac{\varphi_s(\theta)-\varphi_p(\theta)}{2} + \frac{3\pi}{4}. \tag{10}$$

Therefore, the light intensity could be zero and given by

$$I = \sqrt{A^2 + B^2} = 0. \tag{11}$$

Since $r_p(\theta)$, $r_s(\theta)$, $\varphi_p(\theta)$, and $\varphi_s(\theta)$ are all only dependent on the incident angle θ, we can see that α and β are only decided by θ, as shown in Eqs. (6) and (10). Thus with adjustment of polarizer F and K, the light intensity could be zero only at a certain incident angle. Therefore, the application of PI technique results in a lower dip of SPR angular spectrum whose minimum is zero (curve 2 in Fig. 3) than that of the SPR angular spectrum without PI (curve 1 in Fig. 3). In conclusion, the purpose of PI technique is to reduce the noise of the system which is related to the light intensity and thereby to determine the SPR resonance angle more accurately.

It is interesting to note that with adjustment of polarization orientation of F and K in Fig. 2(a), we can actually reduce the intensity to zero at not only the SPR resonance angle (θ_{SPR}) but also at any other nearby angles. Compared with curve 2 in Fig. 3, which is obtained by applying PI technique at the angle of θ_{SPR}, curves 3 and 4 are the SPR angular spectra after applying PI technique at the angles of θ_{SPR} −1° and θ_{SPR} +1°, respectively. It can be seen from Fig. 3 that curve 3 has a narrower width compared with curve 2 and curve 4, which can also help reduce the impact of the noise in determination of the angle affording the minimum intensity.

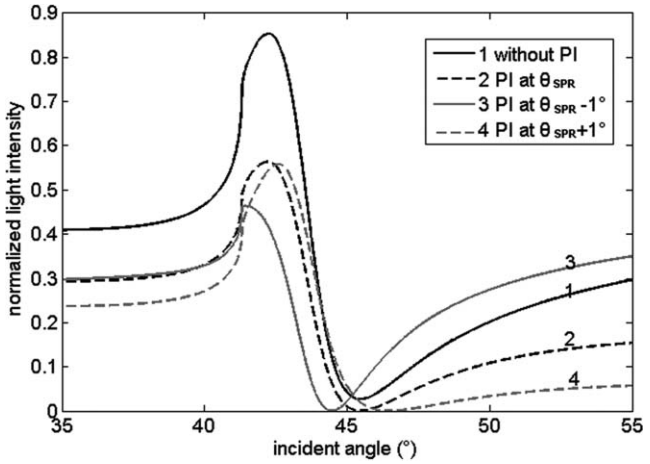

FIG. 3. The simulated effect of polarization interferometry on the SPR angular spectrum. Curve 1 is the original SPR angular spectrum without PI. Curves 2, 3, and 4 are the SPR angular spectrum after applying PI technique at the angles of θ_{SPR}, $\theta_{SPR} - 1^{\circ}$ and $\theta_{SPR} + 1^{\circ}$, respectively, where θ_{SPR} is the angle affording the minimum intensity in curve 1. The simulation is based on Fresnel equations (Ref. 4) and the parameters are a prism of refractive index of 1.515, 2 nm Cr adhesive film, and 30 nm Au film. The dielectric constants of Cr and Au are calculated with Lorentz–Drude model (Ref. 16). The analyte is air whose RI is 1.00026.

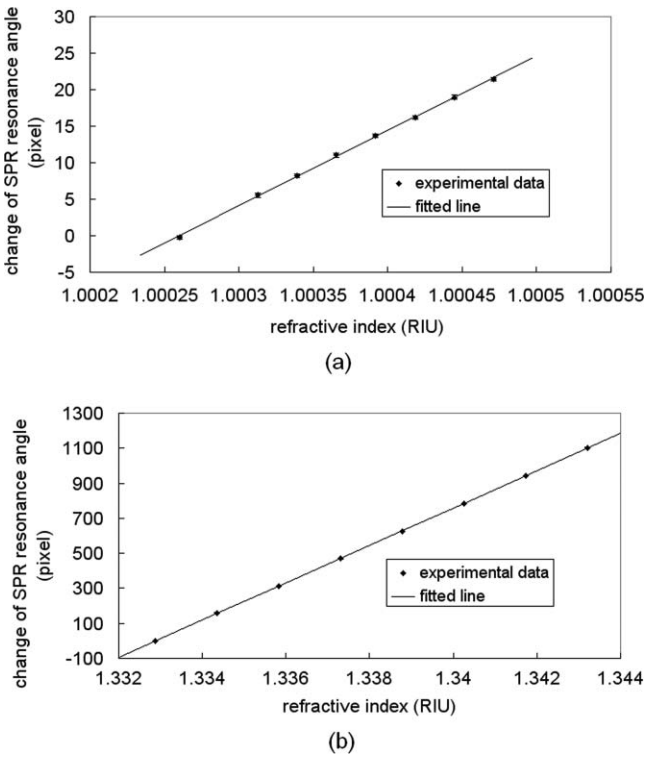

FIG. 4. The result of the sensitivity experiment. The system is held still and used as a one-dimensional sensor and the output of one spot from the sensing line area is used to calculate the following result. (a) The sensor response when the refractive index of the analyte varying from 1.00026 to 1.00047 RIU [air pressure from 0.10 to 0.18 Mpa (Ref. 17)]. Experimental parameters: BK7 glass right angle prism whose RI = 1.515; 2 nm Cr and 40 nm Au films. Error bars show the standard deviation of the sensor output of one spot in 100 s. (b) The sensor response when the refractive index of the analyte varying from 1.33287 to 1.34321 RIU (aqueous solution of sodium chloride with concentrations from 1% to 7%) (Ref. 18). Experimental parameters: ZF6 glass right angle prism whose RI = 1.750; 2 nm Cr and 40 nm Au films. Error bars show the standard deviation of the sensor output of one spot in 100 s.

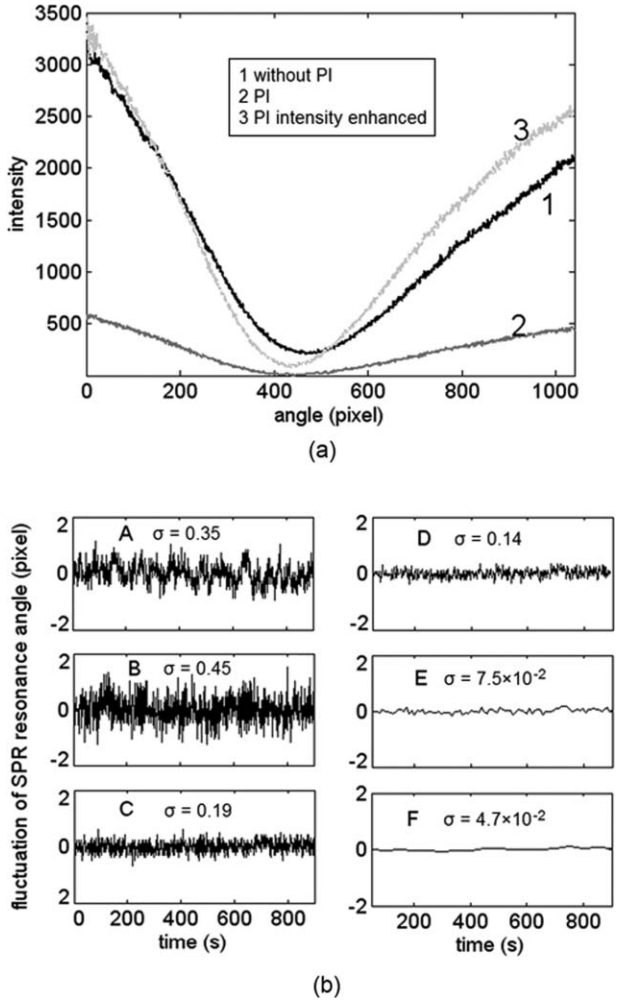

FIG. 5. (a) The SPR angular spectrum of air in the following conditions: curve 1, without PI technique; curve 2, with PI technique, the exposure time of CCD is the same as curve 1; curve 3, with PI technique, the exposure time of CCD is six times as large as curve 1. (b) The fluctuation of SPR resonance angle of one spot in the following conditions: A, without PI technique (standard deviation, $\sigma = 0.35$ pixel); B, with PI technique, the exposure time of CCD is the same as A ($\sigma = 0.45$ pixel); C, with PI technique, the exposure time of CCD is six times as large as A ($\sigma = 0.19$ pixel); D, the same condition with C, two adjacent images averaged ($\sigma = 0.14$ pixel); E, the same condition with C, 10 adjacent images averaged ($\sigma = 7.5 \times 10^{-2}$ pixel); F, the same condition with C, 50 adjacent images averaged ($\sigma = 4.7 \times 10^{-2}$ pixel).

III. PREPARATION OF MICROARRAY

A DNA microarray is manually prepared to test the sensing ability of the system.

Chromium film of ~2 nm thickness and gold film of ~40 nm thickness are coated on a BK7 glass sheet in turn by an ultrahigh vacuum magnetron sputtering coater. The glass sheet with Cr/Au film is immerged in a Piranha solution (3:1 mixture of concentrated sulfuric acid with 30% hydrogen peroxide solution) for 10 min, washed with deionized water, then immerged in acetone solution for 5 min, washed again with deionized water, and dried. A specific segment of Yeast Y5 gene (SH-Oligon-T18 -CTCATGCCCATGCCGATGC) is chosen as our experimental DNA probe. The thiolated probe is purchased from TaKaRa Dalian, China. The DNA probe is dissolved by Milli-Q water and DNA probe solutions with different concentrations are prepared with Tris–NaCl buffer

(10 mM Tris, 100 mM NaCl). The probe solutions are then manually dropped onto the surface of the gold film to form an array. The array of DNA is then immobilized by incubating in a humidity chamber at 37 °C for 6 h. The unimmobilized DNA probes are rinsed off with deionized water.

IV. RESULT AND DISCUSSION

A. Sensitivity, linear range

As introduced in Sec. III, the DNA probes are immobilized on the surface of the Cr–Au film and will be detected in the atmospheric environment. Thus we first test the sensor sensitivity at the refractive index close to 1.0 RIU. We change the refractive index from 1.00026 to 1.00047 RIU by varying the pressure of air. The result is shown in Fig. 4(a). From the slope of the line in Fig. 4(a), we can see that the sensitivity of our SPR sensor is 1.02×10^5 pixel/RIU and is 190°/RIU after converting pixel into degree (°).

To demonstrate the wide linear range of our two-dimensional SPR sensor, we replace the BK7 glass prism (refractive index of 1.515) with a ZF6 glass prism (refractive index of 1.750) and change the sensing analyte for aqueous solution of sodium chloride with different concentrations (corresponding to a different refractive index). We change the refractive index from 1.33287 to 1.34321 RIU and the resulting sensor output is shown in Fig. 4(b). We can see from Fig. 4(b) that the relationship between the resulting sensor output and the refractive index is linear in the range of over 0.01 RIU, and this range is only limited by the pixel numbers of the CCD camera. This wide linear range is useful for applications such as SPR biosensing with magnetic microbeads or monitoring the RI change during a whole biochemical cycle.[19] The SPR sensors with angle interrogation have the superiority of wide linear range compared with SPR sensors with other interrogations.

B. RI resolution

The PI technique is introduced to reduce the noise of the sensor. To evaluate the result of PI, our system is used as a one-dimensional sensor for detecting the RI of air outside the bare gold film. The fluctuations of the sensor outputs with and without PI are compared in one spot of the sensing line area. The SPR angular spectrum curve of air without PI is shown as curve 1 in Fig. 5(a) and the fluctuation of the SPR resonance angle is shown in Fig. 5(b)-A. Curve 2 in Fig. 5(a) is the SPR angular curve of air with PI under the same exposure time, and the fluctuation of SPR resonance angle is shown in Fig. 5(b)-B. Because of the transmittance of polarizer [K in Fig. 2(a)], the intensity of the SPR spectral curve with PI [curve 2 in Fig. 5(a)] is too small, resulting in a worse signal to noise ratio (SNR) [B in Fig. 5(b), standard deviation $\sigma = 0.45$ pixel] than the SNR without PI [A in Fig. 5(b), $\sigma = 0.35$ pixel]. So, we increase the exposure time to enhance the intensity of SPR curve with PI [curve 3 in Fig. 5(a)], and the corresponding fluctuation of SPR resonance angle is shown in Fig. 5(b)-C. It can be seen from Fig. 5(a) that the intensity enhanced SPR angular curve with PI [curve 3 in Fig. 5(a)] has a smaller minimum than that without PI [curve 1 in

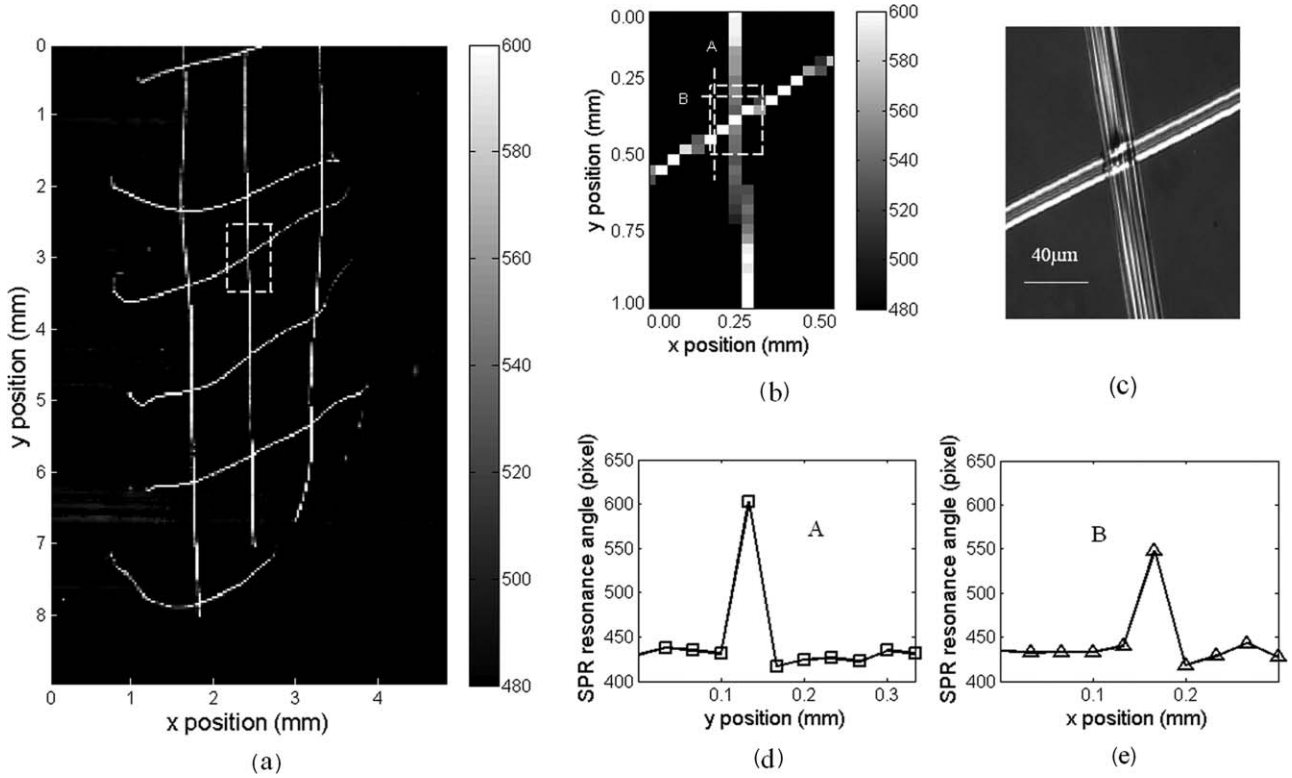

FIG. 6. (a) The sensing result of the gold film scratched by a needle tip. (b) The enlarged marked area in (a). (c) The microscopic picture of the marked square area in (b). [(d) and (e)] Partially plotted column A and row B of (b).

Fig. 5(a)]. This leads to a better noise level [C in Fig. 5(b), $\sigma = 0.19$ pixel] than the one without PI [A in Fig. 5(b), $\sigma = 0.35$ pixel]. In conclusion, the application of PI technique could reduce the noise and thus improve the resolution of the sensor.

The noise of the sensor can also be reduced by averaging adjacent images captured by the CCD. With the same exposure time as Fig. 5(b)-C, the fluctuation of SPR resonance angle with PI after averaging adjacent 2, 10, and 50 images are shown in Fig. 5(b)-D, E, and F and the standard deviations are 0.14, 7.5×10^{-2}, and 4.7×10^{-2} pixel, respectively. This approach could be taken to reduce the noise, but it has to consume more time. So we normally choose two images to average in our measurements.

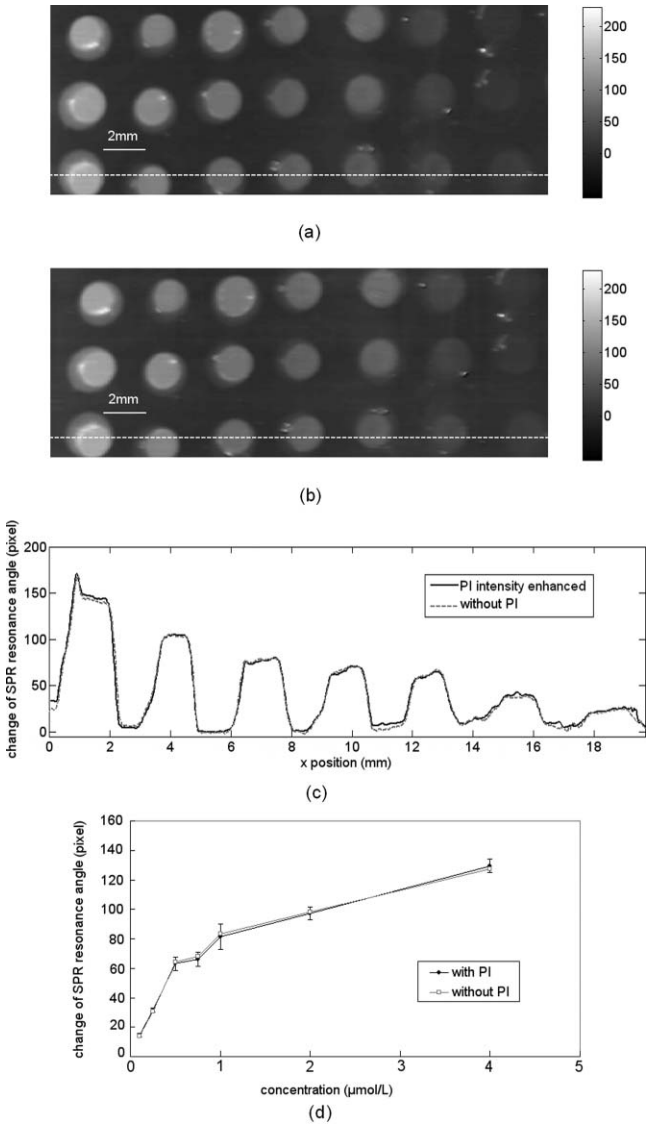

FIG. 7. Detection of DNA microarray. [(a) and (b)] The detection results of a 3 ×7 Yeast Y5 DNA microarray with PI [(intensity enhanced, (a)] and without PI (b) by the system. Three rows have the same distribution: the Yeast Y5 DNA probes prepared with concentration of 4, 2, 1, 0.75, 0.5, 0.25, and 0.1 μM from left to right. Each probe spot is prepared with 0.5 μl probe solution. (c) The plotted dashed rows in (a) and (b). (d) The dependences of the change of SPR resonance angle on the prepared concentrations derived from (a) and (b). Each data is calculated by averaging one probe spot between an upper and a lower limit, the error bars are calculated from three spots with the same concentration in (a) or (b).

To evaluate the sensing resolution of the system, we use the formula reported by Homola[20]

$$\delta n = \frac{\delta O}{S_n}, \tag{12}$$

where δn is the RI resolution of the system, δO is the standard deviation of the sensor output (SPR resonance angle), and S_n is the sensitivity of the system (1.02×10^5 pixel/RIU, calculated in Sec. IV A). Under a normal condition (PI and two images averaged) the standard deviation of the sensor output δO is 0.14 pixel [Fig. 5(b)-D], whereas under a more time-consuming condition (PI and 50 images averaged) the standard deviation of the sensor output δO is 4.7×10^{-2} pixel [Fig. 5(b)-F]. Therefore, the resolution of the system is 1.4×10^{-6} RIU under normal condition and 4.6×10^{-7} RIU under a more time-consuming condition, which is better than other conventional two-dimensional SPR imaging sensors that have been reported.[7,10–12] Considering the much wider linear range, our sensor has a great potential for two-dimensional biosensing applications.

C. Spatial resolution

To test the spatial resolution of the system, a needle tip is used to scratch the sensing plane to get some ultrathin lines on the gold film. Figure 6(a) shows the sensing result of the scratched gold film. The marked square area in Fig. 6(a) is enlarged, as shown in Fig. 6(b). Column A and row B are partially plotted in Figs. 6(d) and 6(e), respectively. It is shown from Figs. 6(d) and 6(e) that the full widths at half-maximum of the scratched line in both transverse and longitudinal orientations are within 1 pixel, which corresponds to a spatial distance of approximate 40 μm. Figure 6(c) is the microscopic picture (objective 40×, DM1000 microscope, Leica) of the marked square area in Fig. 6(b). The widths of the scratched line in transverse and in longitudinal orientations are 34 and 18 μm, respectively. So the spatial resolution of the system is smaller than the spatial distance of 1 pixel, i.e., better than 40 μm. This result is enough for microarray analysis (typical point size 100 μm or larger).

D. Detection of DNA microarray

A Yeast Y5 DNA microarray is fabricated on the gold film with the methods mentioned in Sec. III. Yeast Y5 DNA probes are prepared into a 3 × 7 array with different concentrations of 4, 2, 1, 0.75, 0.5, 0.25, and 0.1 μM from left to right, with the same distribution in each row. Each probe spot is prepared with 0.5 μl probe solution.

Then the Yeast Y5 DNA microarray is detected by our two-dimensional SPR biosensing system. Figures 7(a) and 7(b) show the SPR resonance angle distribution maps of the DNA microarray with PI (intensity enhanced) and without PI technique, respectively. Two dashed rows of Figs. 7(a) and 7(b) are plotted in Fig. 7(c). We can see from Figs. 7(a)–7(c) that the sensing results with and without PI are nearly identical, except that the SPR resonance angle distribution map with PI is a little cleaner because the PI technique makes the sensor less vulnerable to noises. It can also be seen from

Figs. 7(a)–7(c) that the DNA probes can be clearly distinguished and the DNA probes prepared with different concentrations have different SPR resonance angles. From the data in Figs. 7(a) and 7(b), the dependences of SPR resonance angle on the prepared concentrations of DNA probe solution with and without PI are calculated and they too are nearly identical [as shown in Fig. 7(d)].

These experiments show the capability of our two-dimensional SPR sensor for microarray detection. More applications including hybridization of the microarray will be introduced in our further work.

V. CONCLUSION

A two-dimensional polarization interferometry based parallel scan angular SPR biosensing technique is presented. We combine the angle interrogation based SPR sensor and the parallel line scanning into a two-dimensional quantitative SPR sensor, and furthermore, apply the PI technique to reduce the noise. This technique has a refractive index resolution of 1.4×10^{-6} RIU under normal condition (two images averaged) and 4.6×10^{-7} RIU under a more time-consuming condition (50 images averaged). The spatial resolution of this technique is better than 40 μm. The parallel scan method enables the system to detect the refractive index quantitatively with a high throughput. Moreover, our system has a wider dynamic range and a better resolution than the conventional SPR two-dimensional systems. Finally, the good performance in the DNA microarray analysis shows the potential applications of our technique in microarray analysis.

ACKNOWLEDGMENTS

This research was made possible with the financial support from the 863 project, China (Grant No. 2006AA06Z402) and National Science Foundation of China (NSFC), China (Grant No. 30770592 and 61040067).

[1] J. Homola, S. S. Yee, and G. Gauglitz, Sens. Actuators B **54**, 3 (1999).
[2] J. Homola and M. Piliarik, in *Surface Plasmon Resonance Based Sensors*, edited by J. Homola (Springer-Verlag, Berlin, 2006).
[3] J. Homola, Chem. Rev. **108**, 462 (2008).
[4] H. Raether, *Surface Plasmons on Smooth and Rough Surfaces and on Gratings* (Springer, New York, 1988).
[5] B. Rothenhäusler and W. Knoll, Nature (London) **332**, 615 (1988).
[6] E. Fu, T. M. Chinowsky, J. Foley, J. Weinstein, and P. Yager, Rev. Sci. Instrum. **75**, 2300 (2004).
[7] S. Y. Wu, H. P. Ho, W. C. Law, C. L. Lin, and S. K. Kong, Opt. Lett. **29**, 2378 (2004).
[8] C. L. Wong, H. P. Ho, Y. K. Suen, S. K. Kong, Q. L. Chen, W. Yuan, and S. Y. Wu, Biosens. Bioelectron. **24**, 606 (2008).
[9] G. G. Nenninger, M. Piliarik, and J. D. Homola, Meas. Sci. Technol. **13**, 2038 (2002).
[10] T. M. Chinowsky, J. G. Quinn, D. U. Bartholomew, R. Kaiser, and J. L. Elkind, Sens. Actuators B **91**, 266 (2003).
[11] J. S. Yuk, S. J. Yi, H. G. Lee, H. J. Lee, Y. M. Kim, and K. S. Ha, Sens. Actuators B **94**, 161 (2003).
[12] L. Liu, Y. H. He, Y. Zhang, S. H. Ma, H. Ma, and J. H. Guo, Appl. Opt. **47**, 5616 (2008).
[13] A. M. C. Lokate, J. B. Beusink, G. A. J. Besselink, G. J. M. Pruijn, and R. B. M. Schasfoort, J. Am. Chem. Soc. **129**, 14013 (2007).
[14] A. V. Kabashin, V. E. Kochergin, A. A. Beloglazov, and P. I. Nikitin, Biosens. Bioelectron. **13**, 1263 (1998).
[15] Z. L. Sun, Y. H. He, and J. H. Guo, Appl. Opt. **45**, 3071 (2006).
[16] B. Ung, Drude-Lorentz and Debye-Lorentz models for the dielectric constant of metals and water. See http://www.mathworks.com/matlabcentral/fileexchange/18040
[17] J. A. Stone and J. H. Zimmerman, Refractive index of air calculator based on ciddor equation on NIST website. See http://emtoolbox.nist.gov/Wavelength/Ciddor.asp
[18] W. Lu and W. M. Worek, "Two-wavelength interferometric technique for measuring the refractive index of salt-water solutions," Appl. Opt. **32**, 3992–4002 (1993).
[19] Y. Sun, Y. Bai, D. Song, X. Li, L. Wang, and H. Zhang, Biosens. Bioelectron. **23**, 473 (2007).
[20] J. Homola, Sens. Actuators B **41**, 207 (1997).